Stochasticity induced transition from homeostasis to catastrophe

Rudro R. Biswas,^{1,*} Charles S. Wright,^{1,2} Kunaal Joshi,¹ and Srividya Iyer-Biswas^{1,†}

What are the signatures of the onset of catastrophe? Here we present the rich system physics characterizing the stochasticity driven transition from homeostasis to breakdown in an experimentally motivated and analytically tractable minimal model. Recent high-precision experiments on individual bacterial cells, growing and dividing repeatedly in a variety of environments, have revealed a previously unknown intergenerational scaling law which not only uniquely determines the stochastic map governing homeostasis, but also, as we show here, offers quantitative insights into the transition from the "conspiracy principle" regime (homeostasis) to the "catastrophe principle" regime and then to system breakdown. These transitions occur as a single parameter is tuned; we predict the precise values of the parameter which mark the characteristic progression of the transition. Emergence of asymptotically scale invariant distributions with quantifiable power law tails and the reverse monotonicity of the conditional exceedance distribution further characterize the transition to catastrophe.

Catastrophes inspire awe and fear. While wildfires, collapsing bridges, epidemics, avalanches, oil spills, and stock market crashes may conjure dramatically different imagery, this apparent disparity masks underlying recurring themes: the randomness of the triggering event, the systemic breakdown, and the difficulty in restoring the complex system to its previously functional state [1]. These aspects of catastrophes present challenges to effectively modeling them and even to articulating precisely what constitutes a catastrophe. Grappling with the complexity of these systems (their interconnected parts, inherent probabilistic dynamics, and emergent behavior) while capturing the essential phenomenology in a tractable model presents part of the challenge. Another aspect lies in identifying the defining characteristic signatures that predict an impending catastrophe with sufficient precision to facilitate timely intervention before homeostasis is disrupted, rather than just mitigation after the fact.

Homeostasis is routinely conceptualized as a natural outcome of feedback control mechanisms [2, 3]. Within this perspective, the breakdown of homeostasis occurs due to feedback loops malfunctioning or becoming overwhelmed, leading to pathological states [4, 5]. Homeostatic systems can only recover from deviations confined to regions of phase space near the intended equilibrium or basin of attraction [6]. Such temporary disruptions occur when deviations remain within a recoverable range, and feedback mechanisms are delayed or partially effective, but eventually restore homeostasis (e.g., a mild allergic reaction where histamine release causes local swelling that is soon counteracted by anti-inflammatory signals). However, if the system enters a different attractor state, recovery to the original stable point becomes impossible, and the system transitions into an irrecoverable state. When deviations exceed a critical threshold, feedback mechanisms are either overwhelmed (e.g., in anaphylactic shock) or

become positive feedback loops, further destabilizing the system, which can no longer self-correct without external intervention [7]. Whereas systems experiencing temporary disruptions typically exhibit a relatively fast rate of recovery once the perturbation is addressed (e.g., mild dehydration can be corrected by fluid intake), during a breakdown, the system either recovers very slowly or not at all without intervention (e.g., renal failure where dialysis is needed).

But is there a system physics governing the transition from homeostasis to catastrophe? In this work, we leverage knowledge of a recently uncovered scaling law governing stochastic intergenerational homeostasis in single bacterial cells to answer this question. High-precision experiments have revealed the existence of this law and its implications for homeostasis of bacterial cell size across multiple rounds of growth and division. Our approach captures the homeostasis regime's phenomenology precisely—as observed in a naturally occurring complex and adaptive system—and does so in a minimal, analytically tractable model with a single tunable parameter. We examine what this minimal model reveals about the quantitative signatures of the onset of catastrophe as the parameter is tuned. While even simple bacterial cells have many additional layers of control to prevent routine catastrophes, examining the model in the regime where homeostasis is no longer guaranteed provides rich insights into the system physics governing the stochasticity induced transition to catastrophe.

Model and Background

Recent high-precision longterm experiments [8, 9] on individual bacterial cells growing and dividing repeatedly in precisely controlled steady-state conditions have shown that (i) integenerational size evolution is Marko-

¹Department of Physics and Astronomy, Purdue University, West Lafayette, IN 47907, USA

²Monash Biomedicine Discovery Institute, Monash University, Melbourne, Australia

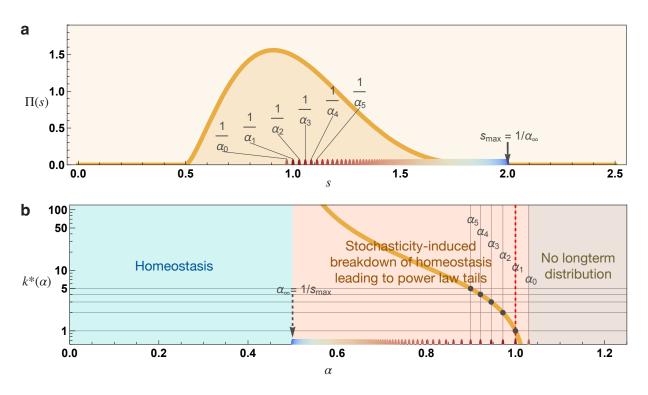


FIG. 1. Stochasticity governs specification of distinct regimes corresponding to: homeostasis, onset of catastrophe, and system breakdown. (a) Shows the model $\Pi(s)$ used for simulations of Eq. (3). It is a beta distribution with parameters (2.5,5) in standard notation, stretched and translated to lie between $s_{\min} = 0.5$ and $s_{\max} = 2$. The mean is 1 as required. (b) Shows three different dynamical regimes that occur as α is varied in Eq. (3). $\alpha = 0$ corresponds to perfect homeostasis of the state variable a. The region of stable homeostasis extends between $0 \le \alpha < \alpha_{\infty} = 1/s_{\text{max}} = 0.5$, where all moments of the long time a-distribution are finite, independent of initial conditions and the distribution itself is characterized by strict bounds, Eq. (16). The regime of stochasticity-induced breakdown of homeostasis extends over $\alpha_{\infty} < \alpha < \alpha_0$, with $\alpha_0 > 1$ (Eq. (7c)), where a long term a-distribution exists but is heavy-tailed. The distribution here is characterized by a scale-invariant power law tail decaying with an α -dependent exponent $-(k^*(\alpha)+1)$ (see Figs. 2 and 3). All moments of order $k^*(\alpha)$ and higher are undefined. $k^*(\alpha)$ is obtained by solving $\alpha_k = \alpha$ for k (Eq. (14)) and is plotted as the orange curve in (b) - this solution exists only within the stochasticity-induced breakdown regime $\alpha_{\infty} < \alpha < \alpha_0$, where it decreases monotonically from $+\infty$ to 0. The values α_k (Eq. (6)) corresponding to integer values of k are indicated on the α -axis in (b), and the corresponding values of $1/\alpha_k$ are indicated in (a). By comparing (a) and (b), it is clear that when $1/\alpha$ lies within the tail region of $\Pi(s)$ in (a), the value of $k^*(\alpha)$ increases rapidly and the size distribution power law tail becomes almost undetectable. When α crosses $\alpha_1 = 1$ (dashed red line), even the mean becomes undefined and this is also when dynamical instability sets in from the deterministic viewpoint. However, the longterm distribution persists till α reaches another point $\alpha_0 \simeq 1.03$, beyond which lies the third and final dynamical regime with no defined longterm distribution.

vian, and (ii) revealed a previously unknown intergenerational scaling law, which in turn specifies a new conceptual framework for stochastic homeostasis that is found to hold across bacterial species, growth conditions and experimental modalities [10–12]. Briefly, denoting by a_n the random variable newborn cell size at the beginning of the n^{th} generation, this scaling law states that the meanrescaled probability distribution of a_{n+1} , conditioned on the value of a_n , is independent of a_n (for all n). Denoting this invariant distribution by Π (with unit mean, by definition), and the conditional mean $\langle a_{n+1} | a_n \rangle$ (i.e., the mean $\langle a_{n+1} \rangle$, given a value of a_n) by the function $\mu(a_n)$, the scaling law can be represented thus:

$$\frac{1}{|\Delta s|} \operatorname{Prob}\left(s < \frac{a_{n+1}}{\mu(a_n)} < s + \Delta s\right) \stackrel{\Delta s \to 0}{=} \Pi(s). \tag{1}$$

Furthermore, over the physiological range accessible by experiments, $\mu(a)$ is found to be well-approximated by a straight line [13]:

$$\mu(a) = \alpha a + \beta. \tag{2}$$

The function $\Pi(s)$ and constants α, β can be obtained from high precision experimental data [8, 9, 11].

These experimental results above are precisely equivalent to the following formulation [10–12]: the intergenerational cell size trajectory evolves according to the following stochastic equation:

$$a_{n+1} = s_n(\alpha a_n + \beta). \tag{3}$$

The $\{s_n\}$ are independent random variables drawn from the same distribution Π (with unit mean) defined in

Eq. (1) and represent the source of (multiplicative) noise. In what follows, we will denote the probability distribution of a_n by the functions P_n . Eq. (3) is difficult to solve for an arbitrary functional form of $\Pi(s)$ except for the case $\alpha = 0$, when the size distribution in any generation n after the initial one is exactly

$$P_n(a) = \Pi(a/\beta)/\beta \quad (\alpha = 0). \tag{4}$$

Thus, when $\alpha = 0$, the size distribution function reaches an initial size-independent steady state in one generation (perfect homeostasis) with mean-rescaled distribution Π .

The stability of size distributions arising from the random walk given by Eq. (3) was analyzed in [11]. Of particular interest in [11] was the existence of (cell size) homeostasis, which is the initial condition-independence and wellbehaved nature of the size distribution after many cell generations (i.e., the longterm size distribution). As we recapitulate below, this analysis revealed a sequence of elegant conditions, Eq. (8), involving α (from Eq. (3)) and moments m_k of the probability distribution Π (Eq. (5)), which simultaneously govern the long term convergence and initial condition-independence of the moments of the long term size distribution. The meeting of all these conditions is equivalent to a single elegant geometric relation, Eq. (9), between α and the upper limit, s_{max} , of the extent of the distribution Π . Under this condition the longterm size distribution is homeostatic, i.e., wellbehaved and initial condition-independent with convergent moments.

From homeostasis we now turn our attention to the breakdown of homeostasis. Fig. 1(b) captures and provides a preview of the rich physics of homeostasis breakdown revealed in this work. The richness of the phenomenology contrasts with the widely-held assumption that cell size homeostasis merely requires that the condition $\alpha < 1$ be met, as deduced previously from straightforward theoretical exercises that have considered many heuristic models, both deterministic and random walks, governing intergenerational cell size evolution [13–25].

The question we focus on in this work can be reformulated as follows: what phenomenologies arise when the strength of the multiplicative noise is increased beyond the threshold beyond which homeostatis breaks (i.e., when Eq. (9) is violated)? As stated above the problem appears to be analytically intractable. However, progress is made possible by making a connection with extant literature on the Kesten process [26], which is related to the one in Eq. (3) through a variable transformation. The Kesten process, since first introduced by Kesten [26] decades ago, has re-appeared in diverse contexts involving complex systems, including earthquakes [27], stochastic optimization algorithms [28], economic and financial markets [29, 30], socioeconomic behaviors [31, 32], and social media usage [33].

We show quantitatively that power law tails emerge as the multiplicative noise strength increases beyond the homeostasis-breaking threshold, and analyze the 'catastrophic' consequences by taking advantage of sophisticated tools from the extant literature on actuarial sciences and heavy-tailed distributions [29, 34–36]. Finally, increasing the noise strength beyond an ultimate limit (for which $\alpha > 1$), a well-defined longterm distribution can no longer be accessed. The random walk represented by the stochastic process of Eq. (3) thus offers an experimentally motivated theoretical model for investigating the stability of stochastic processes as is tuned one-dimensionally from homeostasis to catastrophe to breakdown.

Notation: In what follows, we refer to stochastic variables a_n as the 'system state' or 'state' variable, identifying it with cell size only in contexts relevant to the biological motivation described above.

Results

Emergence of distinct regimes of stochastic dynamics. We now show that three distinct stochasticity-induced dynamical phases arise from the stochastic map Eq. (3). Anticipating their usefulness later on, we define two quantities related to Π , the distribution of the stochastic variables s_n . The first is a general moment function of the distribution Π :

$$m_p = \langle s^p \rangle = \int_0^\infty s^p \Pi(s).$$
 (5)

The argument, p, of the function is the index of the moment and we can take it to be continuously varying and satisfying $p \geq 0$. We will also make the physiologically reasonable assumption that $\Pi(s)$ is nonzero within a finite range $s_{\min} < s < s_{\max}$, with $s_{\min/\max}$ chosen such that the range is the minimum possible. Thus, $m_0 = m_1 = 1$ (normalized probability and unit mean) and as $p \to \infty$, $m_p \to (s_{\max})^p$ from below, i.e., $m_p < (s_{\max})^p$ always. The related second definition is of the function:

$$\alpha_p = (m_p)^{-1/p}, \ p > 0,$$

$$= \lim_{p \to 0+} (m_p)^{-1/p}, \ p = 0.$$
(6)

 α_p is a strictly decreasing function of p, as can be seen from the following argument. Consider two positive numbers, $p_1>p_2,$ and assume that s has nonzero variance (otherwise $s^p=1$ for all p since the mean is one). Since x^{p_1/p_2} is a convex function of x for x>0, using Jensen's inequality, $\langle s^{p_1}\rangle = \left\langle (s^{p_2})^{p_1/p_2}\right\rangle > (\langle s^{p_2}\rangle)^{p_1/p_2}$ and so $\alpha_{p_1}<\alpha_{p_2}.$

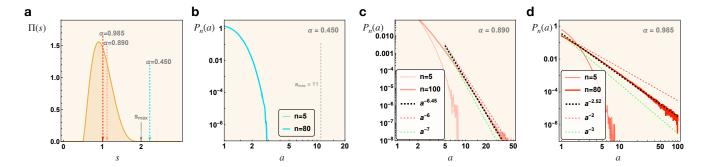


FIG. 2. Emergence of heavy-tailed Pareto power law distributions in the stochasticity induced onset of catastrophe regime. (a) The stretched Beta distribution form used for $\Pi(s)$ in our simulations (Fig. 1(a) has more details). The locations of $1/\alpha$ for the three α values used in (b-2) are indicated by arrows. (b-d) Numerically generated evolution of state variable distributions shown on log-log scale, from generation n=5 to n=80 (b,d) or 100 (c) (long term limit), starting from initial condition $a_0=0.8$ (b,d) or 1.0 (c). The 'target'/long term average of a has been chosen to be unity in all plots. 10-100 million trajectories were simulated for each figure. (b) $\alpha=0.45<0.5=1/s_{\rm max}$ and so strict homeostasis occurs with finite, well-defined initial-condition-independent moments of the long time state variable distribution. There is an upper cutoff, $a_{\rm max}$, that can be analytically calculated (Eq. (16)) and is consistent with the numerical result. (c) α is now increased to satisfy $\alpha_6 < \alpha < \alpha_5$. Thus k=6 (see main text) and the a-distribution is seen to develop a power law tail with exponent $-(k^*(0.89)+1) \simeq -6.45$ lying between -7 and -6. In this case, the sixth and higher moments of the long term distribution are undefined and initial-condition-dependent. (d) α is now large enough that $\alpha_2 < \alpha < 1$ and so even the second moment of the long term a-distribution does not exist. As expected, the heavy tail has a power law decay with the exponent $-(k^*(0.985)+1) \simeq -2.52$ lying between -3 and -2.

It is straightforward to see that

$$\alpha_1 = 1$$
, (Π has unit mean) (7a)

$$\alpha_{\infty} = \lim_{n \to \infty} \alpha_p = 1/s_{\text{max}}, \text{ and}$$
 (7b)

$$\alpha_0 = \lim_{p \to 0+} (m_p)^{-1/p} = e^{-\langle \ln(s) \rangle} > \alpha_1 = 1.$$
 (7c)

We can now pithily describe the stability conditions governing Eq. (3). By explicit evaluation of the intergenerational evolution of the k^{th} $(k=1,2,\ldots)$ moment of the state variable distribution, $\langle (a_n)^k \rangle$, we showed [11] that this k^{th} and all lower moments reach a finite and initial condition-independent longterm value, $\langle a^k \rangle_{\infty}$, if and only if

$$\alpha < \alpha_k$$
. (8)

Furthermore, we show below that this condition along with its implications for convergence of moments hold for all real k over the continuous range $0 \le k < \infty$ and not just when k is a positive integer.

As $k \to \infty$, we obtain the necessary and sufficient condition for all state variable moments to converge to finite initial condition-independent values and ensure existence of a well-behaved initial condition-independent homeostatic distribution [11]:

$$\alpha \le \alpha_{\infty} = 1/s_{\text{max}}.\tag{9}$$

(The equality sign arises from the fact that the α_p are always less than their $p \to \infty$ limit, α_{∞} .) This elegant con-

dition is remarkably consistent with experimental observations of cell size distributions of bacterial cells in homeostasis across growth conditions, experimental modalities and species [8–11].

Remarkably, the stability condition Eq. (8) is also applicable to the stable existence of the k=0 moment in the long term limit, which in turn corresponds to the very existence of a normalizable longterm probability distribution. This can be deduced from the results from a seminal work by Kesten [26]. Kesten's process is a stochastic map of the form:

$$Y_{n+1} = M_n Y_n + Q, (10)$$

where M_n form a series of i.i.d. random variables and Q > 0. As previously mentioned, this process has since re-appeared in diverse contexts involving complex systems, including earthquakes [27], stochastic optimization algorithms [28], economic and financial markets [29, 30], socioeconomic behaviors [31, 32], and social media usage [33]. Using fundamental results from the theory of multiplicative noise, Kesten proved [26] that the longterm distribution exists only when the statistics of the M_n variables ensure that

$$\langle \ln M \rangle < 0. \tag{11}$$

Since Eq. (3) can be recast as Eq. (10) with the identifications $Y_n = a_n + \beta/\alpha$, $M_n = \alpha s_n$, and $Q = \beta/\alpha$, we conclude that the condition for existence of a longterm probability size distribution, Eq. (11), becomes for our

problem:

$$\langle \ln \alpha s \rangle < 0$$
, i.e., $\alpha < e^{-\langle \ln s \rangle} = \alpha_0$, (12)

as claimed. Since $\alpha_0 > 1$ (Eq. (7c)), this upper limit on α for when convergence to a long-term steady state is allowed, is greater than the value of the deterministic threshold for loss of homeostasis (equal to 1).

These stability conditions are visually presented as colorcoded regimes in Fig. 1(b). When $0 \le \alpha < \alpha_{\infty} = 1/s_{\text{max}}$ (blue), there exists a longterm distribution that is stable, initial condition-independent and with finite moments. Increasing α further, α successively crosses the values α_k with decreasing values of k, such that when it lies in the range $\alpha_k \leq \alpha < \alpha_{k-1}$, the k^{th} and higher order moments of a are indeterminate, while all lower order moments reach finite and initial condition-independent longterm values. In the entire range $\alpha_{\infty} < \alpha < \alpha_0$, a longterm distribution is still reached and, as shown next, is characterized by the emergence of a scale-invariant power law tail. We call this the stochasticity-induced breakdown regime (red). Finally, when α increases beyond α_0 (which is greater than 1), the concept of a normalizable longterm distribution needs to be abandoned entirely due to runaway dynamics when all state variable values go to infinity (brown).

Emergent scale invariance in the stochasticityinduced breakdown regime. What universal signature characterizes the region $\alpha_{\infty} < \alpha < \alpha_0$ (the 'stochasticityinduced breakdown' phase in Fig. 1(b)) where a longterm distribution exists vet whose moments higher than a certain order are all undefined/infinite? We show now that it is the emergence of scale invariance in the tail of the state-variable distribution. Consider anew the observation from Eq. (8) that when $\alpha_k \leq \alpha < \alpha_{k-1}$, all k^{th} and higher moments of a are undefined [11]. A possible mechanism for this to occur is that the $a \to \infty$ asymptotic behavior of the long time distribution has a power law tail which falls off slower than $a^{-(k+2)}$ but faster than $a^{-(k+1)}$. This emergent scale-invariance of the tail of the state variable distribution is the defining characteristic of the stochasticity-induced breakdown phase. This scale invariance is also an emergent feature since the input stochastic distribution $\Pi(s)$, that of s_n in Eq. (3), has a finite range and no power law or any other type of heavy tail. Indeed, it has been shown that when the condition in Eq. (11) is met, the long time asymptotic distribution of Y (in Eq. (10), related to a by a linear transformation) has a power law tail [26]. Furthermore, the exponent of this power law tail can also be calculated [37] as a function of α , as we show below. (The possibility that the state variable distribution may have no tail at all is mathematically allowed by these older works but never explicitly discussed; yet it is this homeostasis regime that was of interest in the size regulation problem [10].)

Assume the form $P_{\infty}(a) \simeq N_{\infty}/a^{(1+k^*(\alpha))}$ for the tail of the long term distribution of a, characterized by an α -dependent exponent and overall coefficient N_{∞} . Far into this tail $(a \to \infty)$, the presence of β can be ignored in Eq. (3), which can be replaced by $a_{n+1} \simeq \alpha s_n a_n$. At sufficiently large values, both a_{n+1} and a_n fall within the power law tail region of the probability distribution and so:

$$P_{\infty}(a_{n+1}) \simeq \int ds \Pi(s) \int da_n P_{\infty}(a_n) \delta(a_{n+1} - \alpha s a_n)$$
$$= \int ds \frac{\Pi(s)}{\alpha s} P_{\infty}\left(\frac{a_{n+1}}{\alpha s}\right). \tag{13}$$

Substituting the power law behavior of the tail, $P_{\infty}(a) \simeq N_{\infty}/a^{(1+k^*(\alpha))}$, we find that $k^*(\alpha)$ satisfies:

$$\alpha^{k^*(\alpha)} \int ds \Pi(s) s^{k^*(\alpha)} = 1. \tag{14}$$

In other words, $k^*(\alpha)$ is simply the solution (for k) to the equation $\alpha_k = \alpha$, where α_k is as defined in Eq. (6)! Consider now the straightforward fact that the power law $tail \simeq N_{\infty}/a^{(1+k^*(\alpha))}$ leads to undefined moments $\langle a^p \rangle$ for all real $p \geq k^*(\alpha)$). This fact and the physics underlying Eq. (12) [26] together show that the relationship between the inequalities in Eq. (8) and finiteness of certain moments of a, originally derived only for positive integer values of k, are valid for all real k within the continuous range $0 \leq k \leq \infty$.

Due to the previously derived monotonic decreasing property of α_p as a function of p, if $\alpha_{k+1} \leq \alpha < \alpha_k$, then we also have $k < k^*(\alpha) \le k+1$. As α is increased starting from 0 (perfect homeostasis) but to a value less than $\alpha_{\infty} = 1/s_{\text{max}}$, the system continues to be in homeostasis and Eq. (14) does not have a solution. Homeostasis is broken as α crosses α_{∞} and Eq. (14) becomes solvable (Fig. 1(b)) with $\lim_{\alpha \to \alpha_{\infty} +} k^*(\alpha) = +\infty$. As α increases towards $\alpha_1 = 1$, the point at which the system is no longer stable according to the deterministic arguments, $k^*(\alpha)$ drops from $+\infty$ to 1, the power law tail becomes heavier and more and more of the lower moments of the size distribution (with orders $> k^*(\alpha)$) become undefined. At $\alpha = 1$, the longterm distribution has a tail that falls off as a^{-2} , precluding the existence of a finite and initial condition-independent mean. Yet as α increases further, the longterm distribution continues to exist, though devoid of finite moments at any positive integer order. This remnant of describability using the concepts of stochastic processes also disappears when α approaches α_0 (Eq. (7c)) from below and the distribution tail approaches a^{-1} , which is not normalizable. For $\alpha > \alpha_0$ there is no longterm limit for the state variable distribution to converge to as all values run away to infinity. This description of the evolution of distribution shape with α mirrors the moment-based description provided earlier (also, Fig. 1).

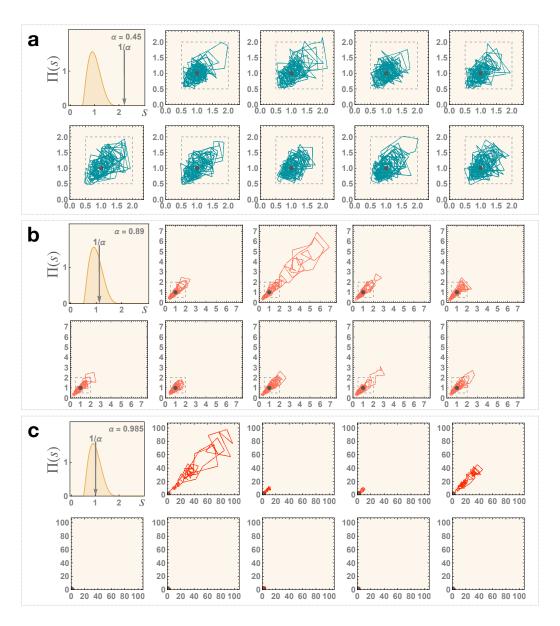


FIG. 3. In the stochasticity induced onset of catastrophe regime giant excursions away from the "set point value" are frequently observed as is typical of the heavy tailed process governing the dynamics in this regime. In each of Fig. (a-c), the first mini-plot provides a visualization for the α -value used in the subfigure by placing $1/\alpha$ on the $\Pi(s)$ graph (same Beta function as used in Fig. 1(a)). The remaining nine mini-plots show independent state variable (a) trajectories as a succession of points (a_n, a_{n+1}) with increasing n, the generation number. Thus, their axes show the next generation a against the current generation value. These axes are normalized by the 'target'/asymptotic average value, $\langle a \rangle_{\infty}$ to facilitate comparison between Figs. (a-c). This target value is also indicated by the gray dot. Each trajectory contains 200 generations. The dashed rectangle is a guide to the eye showing the extent of excursions allowed by variation in s from the target point – as homeostasis is violated, stochastic excursions outside this range becomes more likey. It corresponds the range $(s_{\text{max}}, s_{\text{min}})$ of $\Pi(s)$, the exact boundary limiting excursions when $\alpha = 0$ (see Eq. (4)). (a) When the homeostasis condition, Eq. (9), is satisfied (same as in Fig 2(b)), the a values circulate within/around the marked boundary and have the same order of magnitude as when perfect homeostasis occurs at $\alpha = 0$. Excursions far out are extremely improbable (suppressed exponentially or faster). (b) and (c) show sample trajectories when α violates the stochastic homeostasis condition but not the deterministic stability condition, i.e., $\alpha < 1$. The α -values used in Figs. (b) and (c) correspond to the those in Figs 2(c) and (d), respectively. These now show intermittent giant excursions well outside the marked boundaries. These 'black swan' events characterize heavy tail phenomena, their probabilities falling off slowly as a power law in extent. While there is no characteristic scale describing black swans in this 'scale-invariant' regime, their observed sizes increase with α due to thickening and slowing of the power law tail of the long term a distribution, Fig. 1(b), as occurs here when going from Fig. (b) to (c) (note the axis ranges).

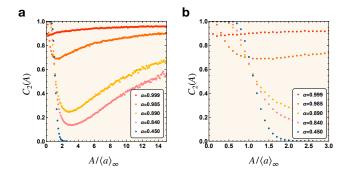
The asymptotic tail of the survival function (one minus the cumulative function, the complementary cumulative distribution function) is thus also a power law, the socalled Pareto power law, with 'Pareto exponent' equal to $-k^*(\alpha)$ (Eq. (14)) in our model. Distributions with such power law tails are of widespread interest and are an important subset of the class of 'heavy-tailed' distributions with remarkable non-intuitive properties which can pose a challenge to conventional strategies for mitigating risk [29, 38]. We have numerically verified the emergence of heavy, power law-tailed longterm distributions from Eq. (3) whose Pareto exponents can be tuned by changing the value of α according to Eq. (14). For simulations we have used a stretched Beta distribution form for $\Pi(s)$ as shown in Fig 1(a), whose range extends between $s_{\min} = 0.5$ and $s_{\max} = 2$. To facilitate comparison between different α , we have used mean-rescaled values for a, dividing them by the mean $\langle a \rangle_{\infty} = \beta/(\alpha-1)$. The decreasing series formed by α_k (with increasing k) starts at 1 for k=1 and decreases to $\alpha_{\infty}=1/s_{\max}=0.5$ as $k \to \infty$. Specific values of α_k corresponding to the distribution in Fig 1(a) are: $\alpha_0 \simeq 1.03$, $\alpha_1 = 1$ (by definition), $\alpha_2 \simeq 0.972, \alpha_3 \simeq 0.946, \dots, \alpha_5 \simeq 0.899, \alpha_6 \simeq 0.879, \dots$ (Fig 1(b)). Thus, in Fig 2(b), well-behaved homeostasis occurs for $\alpha = 0.45 < \alpha_{\infty} = 0.5$, when the mean-rescaled long term distribution is also bounded by a maximum limit $a_{\text{max}}/\langle a \rangle_{\infty} = (1-\alpha)/(1-\alpha s_{\text{max}}) = 11$ (see Eq. (16) below). In the stochasticity-induced breakdown regime, when $\alpha_{k+1} < \alpha < \alpha_k$ for integer k, we expect a power law tail in the longterm distribution with the exponent $-(k^*(\alpha)+1)$ lying in the range -(k+1) and -(k+2). Fig 2(c) and (d) show the cases when $\alpha = 0.89$ and 0.985, for which $k^*(0.89) \simeq 5.45 \ (k=5)$ and $k^*(0.985) \simeq 1.52$ (k=1) respectively. It is clear from the figures that the numerically generated power law tails in the longterm distributions (after ~ 100 generations) have exponents that match the derived values of $-(k^* + 1)$. Furthermore, from our simulations it is clear that as α decreases towards $\alpha_{\infty} = 1/s_{\text{max}}$ and $k^*(\alpha)$ becomes large, these distribution tails fall off sharply, carry lesser total probability weights and become harder to detect. This occurs simultaneously with the value of $1/\alpha$ moving out across the tail of the $\Pi(s)$ distribution, as can be seen from comparing the subfigures in Fig 1. Thus, within the bounds of experimental detection, a homeostatic distribution is guaranteed if $1/\alpha$ is placed outside to the right of the main bulk of the measured Π -distribution, in agreement with the stricter theoretical condition in [11] that $1/\alpha$ should lie to the right of $s_{\rm max}$. In the cell size homeostasis context, this remarkable prediction has indeed been validated experimentally in homeostatic populations for various bacterial species, growth conditions and experimental modalities [8–10].

Emergence of catastrophic events. We now turn our attention to the non-intuitive properties conferred

to state variable distributions within the stochasticityinduced breakdown regime by their scale-invariant tails. In turn, we also highlight the downstream consequences for risk management. To start with, we highlight a visually arresting trend that is evident in the nature of trajectories of the state variable, as shown in Fig. 3. In this figure, we take Π to be the same beta distribution as in Fig. 1(a) and also consider the same three values of α as used in Fig. 2: $\alpha = 0.45$ is located within the homeostasis regime while $\alpha = 0.89$ and 0.985 are in the stochasticityinduced breakdown regime. For each of these values of α , nine random trajectories of the state variable a are numerically generated from Eq. (3) and presented in nextvs-current value plots. The value of a are mean-rescaled by the homeostatic mean $\langle a \rangle_{\infty} = \beta/(1-\alpha)$ for easy comparison across different α values. It is clear that when α is in the regime of homeostasis Fig 3(a) (same value of α as in Fig 2(b)), the trajectories are tightly confined about the mean (gray dot) and limited roughly by the range over which $\Pi(s)$ is nonzero (dashed rectangle; recall from Eq. (4) that at $\alpha = 0$ the mean-rescaled state variable distribution is exactly Π). Any excursions outside these limits are highly suppressed, their probabilities of occurrence falling exponentially or faster with size (defining characteristic of a 'light-tailed' distribution). However, in the heavy-tailed regime ($\alpha = 0.89, 0.985$), the probability of occurrence of a large deviation falls off slowly, as a power law. Thus, intermittent giant excursions of a without any obvious scale of reference (a consequence of the scale-invariant or scale-free nature of the power law tails) can be observed within the modest sample sizes shown in Figs. 3(b) and (c). These catastrophes are popularly known as 'black swan' events [38]. As α approaches the complete breakdown regime, extremely large excursions become more probable (observe how the axis ranges increase from $\alpha = 0.89$, Fig. 3(b), to $\alpha = 0.985$, Fig. 3(c)).

Outlier-driven extremal behavior. Consider when a random sample of N values drawn from a distribution totals to a sum that is extremely large compared to the expected value of N times the distribution mean. When the distribution is a common light-tailed one such as a Gaussian or an Exponential, an analysis of such extremal behavior shows that the most likely method for the large sum to arise is 'conspiratorial' [39–41]. In other words, most of the N variables are larger than the mean by moderate amounts and their cumulative yields the large excess. In contrast, for heavy tailed distributions such extremal behaviors typically involve just one outlier (a 'catastrophe', as viewed from the point of view of traditional contexts where heavy tail analysis is used, such as in finance [29]) which accounts for the excess.

To formulate this concept mathematically, we consider independent random variables $a_1, a_2 \dots a_N$, all identically varying according to the probability distribution under question. The 'catastrophe' principle [39–41]



Outlier-driven extremal population behav-Catastrophic versus conspiratorial. the numerically calculated 2-fold catastrophe measure of the longterm distribution (arising from Eq. (3)), as defined in Eq. (15) with N=2, as a function of the threshold of extremal behavior, A, rescaled by the mean of the state variable, $\langle a \rangle_{\infty}$, for different values of α . These simulations were performed using the Beta function form for $\Pi(s)$ as shown in Fig. 1(a), when $\alpha_{\infty} = 0.5$ divides the Homeostasis regime from the Stochasticity-induced breakdown regime. Thus, $\alpha = 0.45$ lies in the homeostasis regime (Fig. 1(b)) and for this case C_2 can be seen to become zero at large A, showing that the homeostatic distribution satisfies the 'conspiracy' principle. The remaining values of α used are located in the breakdown regime (Fig. 1(b)) and at large A, $C_2(A)$ can be seen to rise towards unity, showing that a single outlier is responsible for the extremal behavior of the sum. Thus, these distributions follow the 'catastrophe' principle, indicating the presence of heavy tails. (b) shows a zoomed-in portion of (a) for small values of mean-rescaled A, showing that C_2 jumps back up to 1 here and the size of this region where it is 1 progressively decreases as α goes up. This occurs because the mean-rescaled lower bound, a_{\min} , of the state of the state variable distribution decreases monotonically with α (Eq. (16)).

obeyed by heavy-tailed distributions states that the distributions of their sum, and their maximum, exhibit the same tail. Thus, for heavy-tailed distributions, the N-fold catastrophe measure

$$C_N(A) = \frac{P(\max(a_1, a_2, \dots, a_N) > A)}{P(a_1 + a_2 + \dots + a_N > A)} \to 1$$
as $A \to \infty$. (15)

Since the event $\max(a_1, a_2, \ldots, a_N) > A$ is a subset of the event $a_1 + a_2 + \ldots + a_N > A$, we always have $\mathcal{C}_N \leq 1$. The fact that \mathcal{C}_N becomes 1 indicates that any exceptional behavior of the collective is almost always the result of a single outlier. This outlier-dominated behavior stands in stark contrast with that of random variables obeying lighter-tailed distributions such as the Gaussian and Exponential distributions, where the ratio above becomes zero as $A \to \infty$ (a 'conspiracy' principle).

In Fig 4, we demonstrate that in the stochasticity-induced homeostasis breakdown regime the distribution of a indeed obeys the catastrophe principle, i.e., outlier

trajectories dominate any extremal behavior of the collective. We have numerically plotted $C_2(A)$ for the mean-rescaled longterm distribution for the case N=2, for α -values encompassing both homeostatic and breakdown regimes. (By iteration, one can show that demonstrating catastrophic behavior in the N=2 case guarantees that such behavior will occur for all N.) In the homeostatic regime, cutoffs exist on both upper and lower ends of the longterm distribution:

$$\frac{a_{\rm m}}{\langle a \rangle_{\infty}} = \frac{1 - \alpha}{1/s_{\rm m} - \alpha}, \quad m = \text{max/min.}$$
 (16)

Thus, in the homeostatic regime, \mathcal{C}_N has to go to zero for large A since the numerator in Eq. (15) becomes zero before the denominator does, as A is increased. This is clearly true in the blue curve in Fig 4 corresponding to the homeostatic regime and indicates the unimportance of outliers there. $a_{\rm max}$ becomes undefined as α crosses $\alpha_{\infty}=1/s_{\rm max}$ into the heavy-tail breakdown regime, where the 'catastrophe' principle comes to play. In this regime, $\alpha>0.5$ in Fig 4, \mathcal{C}_2 is initially less than 1 as it behaves like a light-tailed variable, but as the power-law heavy tail starts exerting influence it picks up and goes towards 1 as expected for outlier-dominated 'catastrophic' behavior. This catastrophe-dominated region of A extends to lower and lower values (of A) as α increases deeper into the homeostatic breakdown regime.

As an aside, in Fig 4 there is a region near A=0 where \mathcal{C}_2 is 1, whose size shrinks to zero as $a\to 1$. This arises because of the existence of a lower cutoff a_{\min} (Eq. (16)), below which the longterm probability distribution vanishes. Thus, $\mathcal{C}_N(A)=1$ for $A< a_{\min}$ since both numerator and denominator in Eq. (15) are identically 1. This region shrinks to zero on the mean-rescaled plot as α increases to 1 because the mean-rescaled a_{\min} monotonically decreases to zero in the interval $0<\alpha<1$, as can be seen from Eq. (16) (also using $s_{\min}<1$).

Reverse monotonicity of the conditional exceedance distribution. A final demonstration of outlier-driven behavior in the stochasticity-induced breakdown regime can be seen by looking at 'filtered' population with state variable values greater than some large value A in the tail of the distribution. What is the nature of distribution of the conditional exceedances [42, 43], $\delta a = a - A$, the amounts by which these values exceed A? Our intuition, based on lighttailed distributions, is that the higher A is, the more squished towards the origin will be this conditional exceedance distribution, and the lesser its mean. When the state variable denotes waiting time, as in queuing theory where the conditional exceedance distribution is called the residual life distribution, this intuition comes from the experience that if one has already waited for a longer time, the remaining wait time will be decreased. This

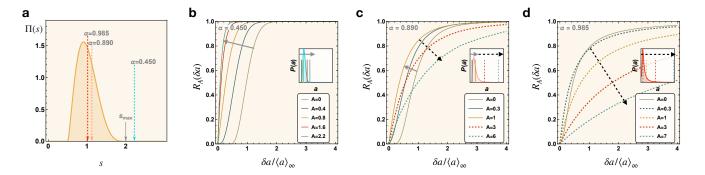


FIG. 5. Reversal of monotonicity of the conditional exceedance distributions in the stochasticity induced onset of catastrophe regime. (a) The stretched Beta distribution form used for $\Pi(s)$ in our simulations (Fig. 1(a) has more details). The locations of $1/\alpha$ for the three α values used in (b-2) are indicated by arrows. (b-d) Numerically generated conditional exceedance distributions (Eq. (17)), $R_A(\delta a)$, corresponding to the longterm cumulative distribution of the conditional exceedance, $\delta a = a - A$, for values of a larger than the threshold A (both mean-rescaled by $\langle a \rangle_{\infty}$). When A is low enough and lies well within the conventional part of the longterm distribution of a (inset), the curves rise up with increasing A (solid arrows). However, when A and a are inside the heavy tail, this ordering with A is reversed (dashed arrows). The insets show the longterm distributions of a: the locations of A-values used are shown and the conventional and heavy-tailed regions indicated by solid/dashed arrows. Since $\alpha = 0.45$ in (b) lies inside the homeostatic regime ($1/\alpha$ is outside to the right of the $\Pi(s)$ distribution in (a); also see Fig. 1(b)), there is only the conventional rising of the curves with A. For $\alpha = 0.89$ (Fig. (c)) inside the breakdown regime, both conventional and heavy tail behaviors can be seen. $\alpha = 0.985$ (Fig. (d)) approaches the complete breakdown regime and so mostly displays heavy-tail behavior.

expectation is however reversed for heavy tailed distributions: larger the threshold A, larger is the probable excess value that will be observed! (In terms of waiting times this translates to the non-intuitive experience: the longer one has waited, the longer one should expect to wait further!)

The conditional exceedance distribution is conveniently characterized by its cumulative distribution function as follows:

$$R_A(\delta a) = P(a < A + \delta a | a > A)$$

$$= \frac{\int_A^{A + \delta a} da P_\infty(a)}{\int_A^\infty da P_\infty(a)}.$$
(17)

Following the discussion above, we expect for light-tailed distributions that the cumulative function $R_A(\delta a)$ will rise to 1 faster for larger A, and so the cumulant curves for larger A will lie above those for smaller A in the $R(A, \delta a)$ vs. δa plots. For heavy tailed distributions, this ordering should be reversed when A is inside the heavy tail region. Fig. 5(b) shows that the conditional exceedance distribution follows the expected light-tailed hierarchy set by the threshold A in the homeostatic regime. In the regime of stochasticity-induced breakdown of homeostasis, however, the heavy tails induce a reversal in this hierarchy (Figs. 5(c), (d)). When the state variable is cell size, this phenomenon can be studied by filtering a synthetic population 'designed' to be in the heavy tail regime through filters of varying sizes and observing the residue of large cells left behind. The mean size of residual individuals in such a population will increase faster than the filter pore size used to filter them.

Discussion

Risk management strategies. The results above provide a multi-faceted characterization of the non-intuitive scalefree extremal behavior exhibited by the longtime distribution in the stochasticity-induced breakdown regime of Eq. (3). We now consider the potential 'economics' associated with such phenomena: the potential costs versus the benefits, in contexts where extremal behavior is costly, such as untenably large sized organisms [8–12], devastating earthquakes [27], or volatile markets [29]. Specifically, what system design principles can help avoid costly catastrophes, while still relaxing the rigidity of control to prevent associated costs from becoming prohibitive. While we highlight the cell size homeostasis problem below, our conclusions can be presumably be applied to other significant contexts, e.g., social and economic scenarios [29, 31] which incorporate processes governed by Eq. (3) (equivalently, Eq. (10)) and where the parameter α may be controlled through, say, rules governing the marketplace and trading behaviors. Equivalently, aspects of $\Pi(s)$ may be controllable, reshaping the function $k^*(\alpha)$ in Fig. 1 and allowing us to achieve the constraints discussed below through an alternate route.

Focusing on control through varying α in Eq. (3), it seems reasonable to assume some benefit of relaxing perfect size control, i.e., having a nonzero large α . For instance, the emergent scaling law, Eq. (1), naturally leads to cell size control through direct size control only over a cell volume reporter species [12], presumably leading to usage of less resources (a benefit) compared when all

components of the cell are monitored to implement perfect control. This reporter-mediated measurement however leads to less control over the cell size (the cost), reflected in a nonzero value for α [12]. Clearly, the complete breakdown region with no longterm distribution, $\alpha > \alpha_0$ (Fig. 1(b)), needs to be avoided since all sizes run away to infinity (thus, there is no normalizable longterm distribution) and result in the maximum cost possible. Further details of system design depend on the nature of this cost-benefit tradeoff, which we discuss in very general terms.

We will assume that the benefit function is finite and after an initial jump after some finite nonzero value of α , quickly saturate or increases very slowly, since using our mechanistic insight above [12] this benefit mainly arises due to changing the nature of size control (direct to indirect) that is responsible. In contrast, the cost of growing too large presumably increases rapidly as a polynomial or exponential in size, saturating if at all at some large value.

When the cost function is exponential in size, it diverges when the size distribution has a power law tail. In this scenario, the entire breakdown region needs to also be avoided, i.e., $\alpha > \alpha_{\infty}$ is forbidden. If the cost function goes as a power law, $\sim a^c$ say, then some flexibility may be allowed. The expected cost, $\sim \langle a^c \rangle_{\infty}$, increases rapidly with α inside the breakdown regime and becomes infinite when α crosses a threshold, α_c , where the power law tail has the exponent -(c+1). This occurs when $k^*(\alpha_c) = c$, where $k^*(\alpha)$ is defined implicitly in Eq. (14) (also, Fig. 1(b)). Minimizing the total cost will thus yield a point $\alpha < \alpha_c$, which lies in the homeostatic regime or well before α_c inside the stochasticity-induced breakdown regime in Fig. 1(b), depending on details.

As previously mentioned, experiments performed at different growth conditions with different bacterial species and across different experimental modalities [8–11], have been found to yield values of α that always lie inside the homeostatic regime and near the transition to breakdown. Experimentally, this is the observation that $1/\alpha$ lies just outside to the right of the experimentally measured $\Pi(s)$. From the foregoing discussion, it then appears that the cost associated with catastrophically large cell sizes is an exponentially growing function or a polynomially increasing function with a large exponent (as seen in Fig. 1, if $1/\alpha$ lies in the experimentally undetectable tail, then α is near α_k values with very large k).

Concluding remarks

We have previously shown [12] the robust architectural underpinnings of the observed emergent simplicities in the stochastic intergenerational homeostasis of individual bacterial cells, including the scaling law Eq. (1) [8]. We have also argued that such emergent simplicities [8, 44] serve as constraints that deconstrain [10, 45, 46]: the diversity of their system-specific implementations, say in different microorganisms or growth conditions, contrasts sharply with the universality of their behaviors as characterized by emergent simplicities [8, 44]. In turn, these behaviors are derived from commonalities in the underlying architecture [10, 12, 47]. By constraining or limiting variations that may break the core functional architecture, these constraints that deconstrain facilitate evolvability. Thus excursions can still occur without catastrophic loss of core functionality [45, 46, 48]. Within this perspective, perhaps the utility of accessing the onset of catastrophe regime becomes apparent under stressful or inclement conditions, when 'black swan' excursions such as in Fig. 3 may provide a route to survival, despite the catastrophic risks. The clustering of observed values of α in homeostatic cells near the boundary which characterizes the onset of catastrophe [9–11] reflects the proximity to the exploratory frontier even when conditions are favorable.

Heavy-tailed distributions are conventionally thought of as being generated through stochastic processes that effectively already incorporate similar heavy-tailed distributions into their prescriptions (Lévy flights, infinite node Poisson model, etc.) [34–36]. Remarkably, we see that the stochastic process considered in this work, Eq. (3), which describes homeostasis in experimentally observed systems [8–12], also generates heavy tailed distributions while maintaining two simple attributes: (i) Its stochasticity arises from a single well-behaved stochastic variable s, and (ii) it allows one-dimensional tuning all the way from well-behaved homeostasis, through a stochasticity-induced breakdown regime described by heavy-tailed distributions with predictable and, in principle, any Pareto exponent value, to a compete breakdown regime berefy of any notion of stability (Fig. 1).

Eq. (3) represents a minimal model of a stochastic process which is tunable across a the complete spectrum of stable, heavy-tailed or completely unstable behaviors, and furthermore is analytically tractable. Eq. (3) is also directly related to Kesten's process, which has been speculated to be relevant for a plethora of real world complex systems, including those involving earthquakes [27], economic and financial markets [29], socioeconomic behaviors [31]. How the insights from this work can inform studies of onset of catastrophes and risk management in these more complex systems remains to be seen.

Acknowledgements: R.R.B. and S.I.-B. gratefully acknowledge Purdue University Startup funds and the Pur-

due Research Foundation for supporting the collaboration and the research. S.I.-B. thanks the Purdue College of Science Dean's Special Fund and the Showalter Trust for partial support. K.J. and S.I.-B. acknowledge support from the Ross-Lynn Fellowship award and the Bilsland Dissertation Fellowship award. R.R.B. and S.I.-B. thank Mogens Jensen for helpful discussions.

Author Contributions: RRB and SI-B conceived of and designed the research; RRB and SI-B derived the theory results and performed numerical simulations; KJ provided the argument for monotonicity of α_p stated between Eqs. (6) and (7); RRB, CSW and SI-B wrote the paper; all authors discussed the results.

- * rrbiswas@purdue.edu
- † iyerbiswas@purdue.edu
- [1] J. H. Miller, A crude look at the whole (Basic Books, New York, 2016).
- [2] N. Wiener, Cybernetics, 2nd ed. (The MIT Press, Cambridge, MA, 1961).
- [3] D. S. Ramsay and S. C. Woods, Physiological regulation: How it really works, Cell Metabolism 24, 361 (2016).
- [4] M. E. Kotas and R. Medzhitov, Homeostasis, inflammation, and disease susceptibility, Cell **160**, 816 (2015).
- [5] N. Wiener, Homeostasis in the individual and society, Journal of the Franklin Institute **251**, 65 (1951).
- [6] K. G. Murphy and N. S. Jones, Quantitative approaches to energy and glucose homeostasis: machine learning and modelling for precision understanding and prediction, J. R. Soc. Interface. 15, 20170736 (2018).
- [7] H. F. Nijhout, J. Best, and M. C. Reed, Escape from homeostasis, Mathematical Biosciences 257, 104 (2014).
- [8] K. Joshi, C. S. Wright, K. F. Ziegler, E. M. Spiers, J. T. Crosser, S. Eschker, R. R. Biswas, and S. Iyer-Biswas, Emergent simplicities in stochastic intergenerational homeostasis, bioRxiv:2023.01.18.524627 10.1101/2023.01.18.524627 (2023).
- [9] K. F. Ziegler, K. Joshi, C. S. Wright, S. Roy, W. Caruso, R. R. Biswas, and S. Iyer-Biswas, Scaling of stochastic growth and division dynamics: A comparative study of individual rod-shaped cells in the mother machine and schemostat platforms, Molecular Biology of the Cell 35:ar78, 1 (2024).
- [10] C. S. Wright, K. Joshi, R. R. Biswas, and S. Iyer-Biswas, Emergent simplicities in the living histories of individual cells, arXiv:2404.01682 (2024), (In press, Annual Review of Condensed Matter Physics).
- [11] K. Joshi, R. R. Biswas, and S. Iyer-Biswas, Intergenerational scaling law determines the precision kinematics of stochastic individual-cell-size homeostasis, bioRxiv:2023.01.20.525000 (2023).
- [12] K. Joshi, C. S. Wright, R. R. Biswas, and S. Iyer-Biswas, Architectural underpinnings of stochastic intergenerational homeostasis, Phys. Rev. E 110, 024405 (2024).
- [13] S. Jun and S. Taheri-Araghi, Cell-size maintenance: Universal strategy revealed, Trends in Microbiology 23, 4 (2015).
- [14] L. Willis and K. C. Huang, Sizing up the bacterial cell

- cycle, Nature Reviews Microbiology 15, 606 (2017).
- [15] S. Modi, C. A. Vargas-Garcia, K. R. Ghusinga, and A. Singh, Analysis of noise mechanisms in cell-size control, Biophys. J. 112, 2408 (2017).
- [16] J. Lin and A. Amir, The effects of stochasticity at the single-cell level and cell size control on the population growth, Cell Syst. 5, 358 (2017).
- [17] M. M. Logsdon, P.-Y. Ho, K. Papavinasasundaram, K. Richardson, M. Cokol, C. M. Sassetti, A. Amir, and B. B. Aldridge, A parallel adder coordinates mycobacterial cell-cycle progression and cell-size homeostasis in the context of asymmetric growth and organization, Current Biology 27, 3367 (2017).
- [18] J. T. Sauls, D. Li, and S. Jun, Adder and a coarse-grained approach to cell size homeostasis in bacteria, Current opinion in cell biology 38, 38 (2016).
- [19] S. Taheri-Araghi, S. Bradde, J. T. Sauls, N. S. Hill, P. A. Levin, J. Paulsson, M. Vergassola, and S. Jun, Cell-size control and homeostasis in bacteria, Current Biology 25, 385 (2015).
- [20] M. Deforet, D. van Ditmarsch, and J. B. Xavier, Cellsize homeostasis and the incremental rule in a bacterial pathogen, Biophysical journal 109, 521 (2015).
- [21] A. Amir, Cell size regulation in bacteria, Physical Review Letters 112, 208102 (2014).
- [22] T. W. Spiesser, C. Müller, G. Schreiber, M. Krantz, and E. Klipp, Size homeostasis can be intrinsic to growing cell populations and explained without size sensing or signalling, The FEBS Journal 279, 4213 (2012).
- [23] P. Nurse, A long twentieth century of the cell cycle and beyond, Cell 100, 71 (2000).
- [24] J. J. Tyson, Size control of cell division, Journal of Theoretical Biology 126, 381 (1987).
- [25] P. Fantes and P. Nurse, *The cell cycle* (Cambridge University Press, 1981) Chap. 2.
- [26] H. Kesten, Random difference equations and renewal theory for products of random matrices, Acta Mathematica 131, 207 (1973).
- [27] Q. Lei and D. Sornette, A stochastic dynamical model of slope creep and failure, Geophysical Research Letters 50, e2022GL102587 (2023).
- [28] P. Diaconis and D. Freedman, Iterated random functions, SIAM Review 41, 45 (1999).
- [29] B. Finkenstadt and H. Rootzén, Extreme values in finance, telecommunications, and the environment (CRC Press, 2003).
- [30] C. Francq, B. M. Kandji, and J.-M. Zakoian, Inference on garch-midas models without any small-order moment, Econometric Theory, 1 (2023).
- [31] X. Gabaix, Zipf's law for cities: An explanation, The Quarterly Journal of Economics 114, 739 (1999).
- [32] T. Boppart, P. Krusell, and J. Olsson, Who should work how much?, Working Paper 32977 (National Bureau of Economic Research, 2024).
- [33] J. J. Jiang, K. Yamada, H. Takayasu, and M. Takayasu, Scale-dependent power law properties in hashtag usage time series of weibo, Scientific Reports 13, 22298 (2023).
- [34] S. I. Resnick, Heavy-tail phenomena: probabilistic and statistical modeling (Springer Science & Business Media, 2007).
- [35] B. B. Mandelbrot, Chapter 1 heavy tails in finance for independent or multifractal price increments, in *Hand-book of Heavy Tailed Distributions in Finance*, Hand-books in Finance, Vol. 1, edited by S. T. Rachev (North-

- Holland, Amsterdam, 2003) pp. 1-34.
- [36] B. B. Mandelbrot, *The fractal geometry of nature* (WH freeman New York, 1982).
- [37] C. M. Goldie, Implicit renewal theory and tails of solutions of random equations, The Annals of Applied Probability 1, 126 (1991).
- [38] N. N. Taleb, Statistical consequences of fat tails: Real world preasymptotics, epistemology, and applications, arXiv:2001.10488 (2020).
- [39] A. Wierman, Catastrophes, conspiracies, and subexponential distributions (part ii) (2013).
- [40] J. Nair, A. Wierman, and B. Zwart, The fundamentals of heavy tails: Properties, emergence, and estimation (Cambridge University Press, 2022).
- [41] X. Wang and C.-H. Rhee, Importance sampling strategy for heavy-tailed systems with catastrophe principle, in 2023 Winter Simulation Conference (WSC) (2023) pp. 76–90.
- [42] M. C. Bryson, Heavy-tailed distributions: properties and tests, Technometrics 16, 61 (1974).

- [43] A. Naess, O. Gaidai, and O. Karpa, Estimation of extreme values by the average conditional exceedance rate method, Journal of Probability and Statistics 2013, 797014 (2013).
- [44] S. Iyer-Biswas, C. S. Wright, J. T. Henry, K. Lo, S. Burov, Y. Lin, G. E. Crooks, S. Crosson, A. R. Dinner, and N. F. Scherer, Scaling laws governing stochastic growth and division of single bacterial cells, Proc. Natl. Acad. Sci. U.S.A. 111, 15912 (2014).
- [45] M. Kirschner and J. Gerhart, Evolvability, Proc. Natl. Acad. Sci. U. S. A. 95, 8420 (1998).
- [46] J. C. Doyle and M. Csete, Architecture, constraints, and behavior, Proc. Natl. Acad. Sci. U. S. A. 108 Suppl 3, 15624 (2011).
- [47] S. Iyer-Biswas, G. E. Crooks, N. F. Scherer, and A. R. Dinner, Universality in stochastic exponential growth, Phys. Rev. Lett. 113, 028101 (2014).
- [48] M. E. Csete and J. C. Doyle, Reverse engineering of biological complexity, Science 295, 1664 (2002).